

Spectral Analysis of the Stromlo-APM Survey II. Galaxy luminosity function and clustering by spectral type

J. Loveday¹, L. Tresse² and S. Maddox^{3,4}

¹*Department of Astronomy and Astrophysics, University of Chicago, 5640 S. Ellis Ave, Chicago, IL 60637, USA*

²*Istituto di Radioastronomia del CNR, Via P. Gobetti, 101, 40129 Bologna, Italia*

³*Institute of Astronomy, Madingley Road, Cambridge, CB3 0HA, UK*

⁴*School of Physics and Astronomy, University of Nottingham, Nottingham, NG7 2RD, UK*
loveday@oddjob.uchicago.edu, tresse@ira.bo.cnr.it, sjm@ast.cam.ac.uk

22 July 2021

ABSTRACT

We study the luminosity function and clustering properties of subsamples of local galaxies selected from the Stromlo-APM survey by the rest-frame equivalent widths of their H α and [O II] emission lines. The b_J luminosity function of star-forming galaxies has a significantly steeper faint-end slope than that for quiescent galaxies: the majority of sub- L^* galaxies are currently undergoing significant star formation. Emission line galaxies are less strongly clustered, both amongst themselves, and with the general galaxy population, than quiescent galaxies. Thus as well as being less luminous, star-forming galaxies also inhabit lower-density regions of the Universe than quiescent galaxies.

Key words: cosmology: observations — galaxies: clustering — galaxies: luminosity function, mass function — surveys

1 INTRODUCTION

Important clues to the physics of galaxy formation and evolution may be obtained by studying the global properties, such as the luminosity function and correlation function, of quiescent versus star-forming galaxies. The most reliable tracer of the formation rate of massive, hot stars is the flux of the H α emission line, directly related to the stellar UV (< 912 Å) photoionizing flux (Kennicutt 1983). This line is frequently redshifted out of the observed spectral window, and so most deep galaxy surveys have instead used the [O II] 3727Å line as a measure of star-formation rate (Kennicutt 1992).

The luminosity function of galaxies subdivided by the presence or absence of the [O II] emission line has been calculated in the local Universe for the Las Campanas Redshift Survey (LCRS, Lin et al. 1996a) and for the ESO Slice Project (ESP, Zucca et al. 1997). In both surveys it was found that the faint-end of the galaxy luminosity function is dominated by [O II] emitters, in other words that presently star-forming galaxies tend to be less luminous than quiescent galaxies in both the b_J (ESP) and Gunn- r (LCRS) bands. These results from [O II]-selected samples are consistent with the recent luminosity function estimates from local samples of galaxies selected by morphological (eg. Marzke et al. 1998) and spectral (eg. Bromley et al. 1998, Folkes et al. 1999) type: early-type (elliptical and lenticular) galax-

ies tend to be luminous, and late-type (spiral and irregular) galaxies faint.

It is by now also well known (eg. Davis & Geller 1976, Giovanelli et al. 1986, Iovino et al. 1993, Loveday et al. 1995) that galaxies of early morphological type cluster together on small scales more strongly than late-type galaxies. Since emission-line galaxies (ELGs) tend to be of late Hubble type, we would expect ELGs to be more weakly clustered than non-ELGs, and indeed this has been observed by numerous authors (eg. Iovino et al. 1988, Salzer 1989, Rosenberg, Salzer & Moody 1994 and Lin et al. 1996b).

In this paper we study the luminosity function and clustering for subsamples of the Stromlo-APM survey (Loveday et al. 1996) selected by H α and [O II] emission-line equivalent widths. The Stromlo-APM survey is ideal for quantifying the statistical properties of emission-line versus quiescent galaxies in the local universe since it contains a representative sample of different galaxy types and covers a large volume $V \approx 1.38 \times 10^6 h^{-3} \text{Mpc}^3$. Since the red wavelength coverage of Stromlo-APM spectra extends from 6300–7600 Å we are able to detect the H α (6562.82Å) line, when present, to a redshift $z \lesssim 0.16$, i.e. beyond the maximum distance reached by the survey. Thus for the first time we are able to classify a large, representative sample of galaxies by the primary tracer of massive star formation, viz. the equivalent width of the H α emission line. Measurement of the spectral properties of Stromlo-APM galaxies is discussed by Tresse et

al. (1999), hereafter referred to as Paper 1. The subsamples selected by their emission-line properties are described in §2. The luminosity functions of the different samples are compared in §3 and in §4 we present clustering measurements. We summarize our results in §5. Throughout, we assume a Hubble constant of $H_0 = 100h \text{ km s}^{-1} \text{ Mpc}^{-1}$ with $h = 1$ and a deceleration parameter $q_0 = 0.5$. The exact cosmology assumed has little effect at redshifts $z \lesssim 0.15$.

2 GALAXY SAMPLES

Our sample of galaxies is taken from the Stromlo-APM redshift survey which covers 4300 sq-deg of the south galactic cap and consists of 1797 galaxies brighter than $b_J = 17.15$ mag. The galaxies all have redshifts $z < 0.145$, and the mean is $\langle z \rangle = 0.051$. A detailed description of the spectroscopic observations and the redshift catalog is published by Loveday et al. (1996).

Of the 1797 galaxies originally published in the redshift survey, 82 have $b_J < 15$. These bright galaxies are excluded from our analysis since they tend to be saturated on the Schmidt plates and hence have unreliable magnitudes. Of the remaining 1715 galaxies, 26 have a redshift taken from the literature, and for 7 we could not retrieve the spectra because they were not observed with the Dual-Beam Spectrograph (DBS) of the ANU 2.3-m telescope at Siding Spring. Also excluded were 6 blueshifted spectra, 3 with $cz < 1000 \text{ km s}^{-1}$, and 2 with too low signal-to-noise.

The remaining 1671 spectra were flux-calibrated and had their spectral properties measured as described in Paper 1. Flux calibration of our spectra is accurate to $\sim 10\text{--}20\%$, and so in the present paper we have restricted our analysis to galaxy samples selected by the equivalent widths (EWs) of their $H\alpha$ and $[\text{O II}]$ emission lines, which are insensitive to flux calibration errors. Note that since the resolution of our spectra has $\text{FWHM} = 5\text{Å}$, the $H\alpha$ line can always be deblended from the $[\text{N II}]$ doublet.

Of the 1671 measured galaxies, 11 were not part of our core statistical sample, either because they had an uncertain redshift or happened to lie in a part of the sky masked by “holes” around bright stars, etc. Of the remaining 1660 galaxies, 82 could not have $\text{EW}(H\alpha)$ measured as their redshift places the $H\alpha$ line in a small gap in the red part of the spectrum from $7000\text{--}7020\text{Å}$ (Loveday et al. 1996). For an additional 57 spectra, $H\alpha$ was seen in emission but could not be measured due to contamination by a sky line, or some other problem with the spectrum; $[\text{O II}]$ lines could not be measured for similar reasons for 5 spectra. Note that lack of EW measurement, while correlated with redshift, is uncorrelated with galaxy morphology, and so we can reliably correct for missing EW measurements. We are thus left with a sample of 1521 galaxies which could be analysed by $\text{EW}(H\alpha)$, and 1655 which could be analysed by $\text{EW}([\text{O II}])$. Histograms of $\log \text{EW}(H\alpha)$ and $\log \text{EW}([\text{O II}])$ are plotted in Figures 1 and 2 respectively.

We select galaxy subsamples using measured equivalent widths of the $H\alpha$ and $[\text{O II}]$ emission lines. The $H\alpha$ line is the best tracer of massive star formation (Kennicutt 1983) but we also select samples using the equivalent width of the $[\text{O II}]$ line, as this line allows us to compare with other surveys in which $H\alpha$ is not always within the wavelength range

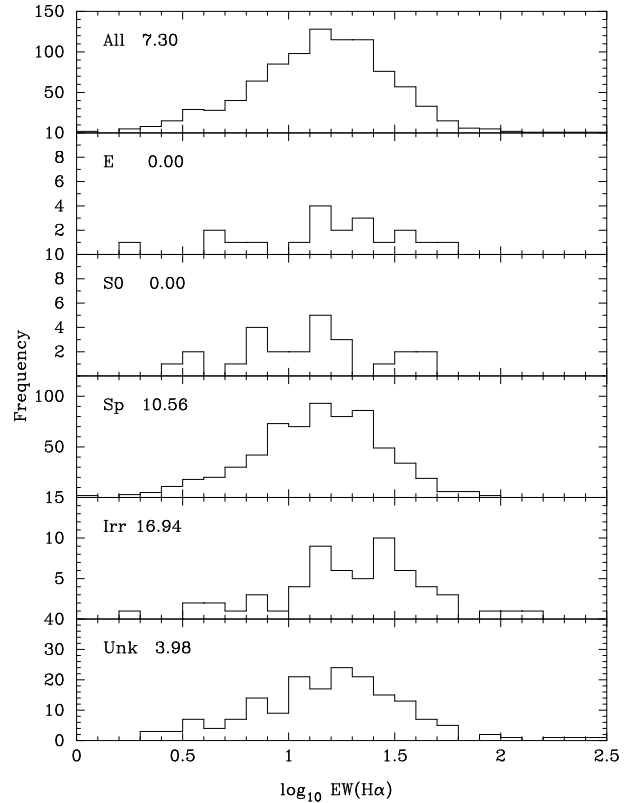


Figure 1. Histogram of $\log \text{EW}(H\alpha)$ for all galaxies and for morphologically selected subsamples as labeled. Note that galaxies with no detected $H\alpha$ are not shown here. The median $\text{EW}(H\alpha)$, including non-detections, is given for each sample after the morphological type.

measured. The $H\alpha$ line is detected with $\text{EW} \geq 2\text{Å}$ in 61% of galaxies. Of these emission-line galaxies, half have $\text{EW}(H\alpha) > 15\text{Å}$. Thus we form three subsamples of comparable size by dividing the sample at $\text{EW}(H\alpha)$ of 2Å and 15Å . In the case of the $[\text{O II}]$ line, 60% of galaxies have $\text{EW} \geq 2\text{Å}$, and of these half have $\text{EW}([\text{O II}]) \geq 9.6\text{Å}$. The galaxy samples selected by $H\alpha$ and $[\text{O II}]$ equivalent widths are defined in Table 1.

Most galaxies in the Stromlo-APM survey have had a morphological type (elliptical, lenticular, spiral or irregular) assigned by visual inspection of the galaxy image (Loveday 1996, Loveday et al. 1996). In Table 1 we give the numbers of galaxies of each morphological type in each spectroscopically selected subsample. In Figures 1 and 2 we also plot the distribution of equivalent widths for these morphologically-selected subsamples. The sample labeled “Unk” consists of galaxies to which no morphological classification was assigned. We see that early-type galaxies dominate when $H\alpha$ or $[\text{O II}]$ emission is not detected and are underrepresented when emission lines are detected. Conversely, the number of irregular galaxies increases significantly in the spectroscopic samples which show strongest star formation. Strong star formation is known to disrupt the regularity in the shape of a galaxy. In the deeper universe, the apparent in-

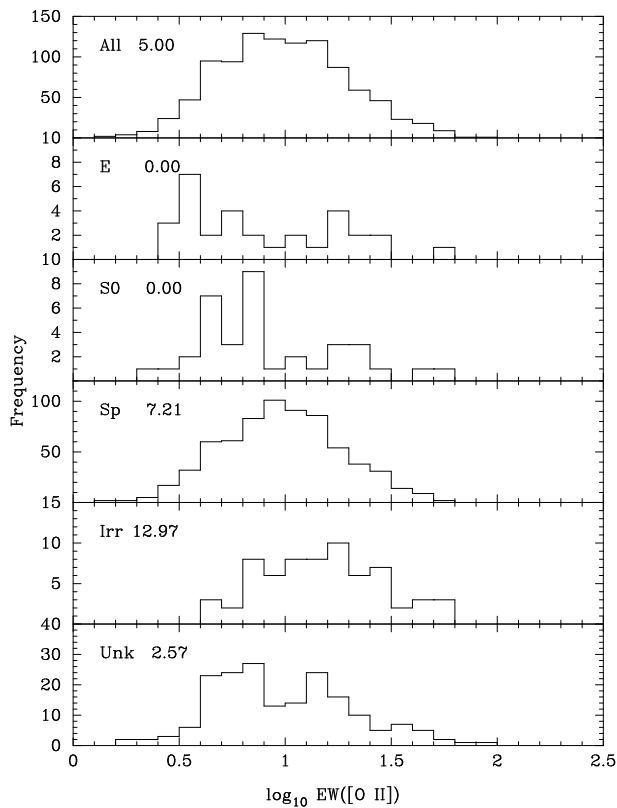


Figure 2. Histogram of \log EW ([O II]) for all galaxies and for morphologically selected subsamples as labeled. Note that galaxies with no detected [O II] are not shown here. The median EW ([O II]), including non-detections, is given for each sample after the morphological type.

Table 1. Spectroscopic subsamples and correlation with morphological type.

Sample	EW (H α)	E	S0	Sp	Irr	Unk	Total
(a) H-low	< 2 Å	125	108	207	10	149	599
(b) H-mid	2–15 Å	8	16	340	18	81	463
(c) H-high	> 15 Å	11	9	303	41	95	459
Sample	EW ([O II])	E	S0	Sp	Irr	Unk	Total
(d) O-low	< 2 Å	120	112	239	8	177	656
(e) O-mid	2–9.6 Å	19	24	344	19	97	503
(f) O-high	> 9.6 Å	12	12	339	47	86	496

crease in number of irregulars is also related to strong star formation (Brinchmann et al. 1998). Thus as expected we find a good correlation between morphological types and emission line equivalent widths. Since they can be measured objectively, spectroscopic properties of galaxies are a more reliable discriminator than visually assigned morphological types. Moreover, a significant fraction of Stromlo-APM

galaxies have no morphological type assigned (the column marked “Unk” in Table 1). The low median EW (H α) and EW ([O II]) for these unclassified galaxies compared with the total sample suggests that many are in fact of early morphological type. The spectral classification described in this section allows these galaxies to be assigned to their appropriate class in a quantitative way.

3 THE GALAXY LUMINOSITY FUNCTION

We estimate the b_J luminosity function (LF) for each galaxy subsample using maximum-likelihood, density-independent methods, so that our results are unbiased by galaxy clustering. We use the Sandage, Tammann & Yahil (1979) parametric maximum-likelihood estimator to fit a Schechter (1976) function,

$$\phi(L)dL = \phi^* \left(\frac{L}{L^*}\right)^\alpha \exp\left(\frac{-L}{L^*}\right) dL. \quad (1)$$

We correct for random errors in our magnitudes by convolving this luminosity function with a Gaussian with zero mean and rms $\sigma_m = 0.30$ (see Loveday et al. 1992, hereafter L92, for details). We also perform a non-parametric fit to each luminosity function using the stepwise maximum-likelihood estimator of Efstathiou, Ellis & Peterson (1988). This estimator calculates $\phi(L)$ in a series of evenly-spaced magnitude bins and provides a reliable error estimate for each bin by inverting the information matrix. K -corrections are applied to each galaxy according to its morphological classification as E/S0: 4.14 z , Sp: 2.25 z , Irr: 1.59 z , Unk: 2.90 z .

Before calculating the LF for each spectroscopic subsample defined in Table 1, we first checked that the galaxies omitted from this analysis, ie. those galaxies whose H α or [O II] emission lines could not be measured, did not bias the LF measurement relative to the full Stromlo-APM survey. The LF estimates using all galaxies except the 194 with no H α measurement available and all galaxies except the 60 with no [O II] measurement were indeed both consistent with the full sample.

Our estimates of the luminosity function for the EW (H α) selected samples are shown in Figure 3. The inset to this Figure shows the likelihood contours for the best-fit Schechter parameters α and M^* . The Schechter parameters and their 1σ errors (from the bounding box of the 1σ error contours) are also listed in Table 2. Note that the estimates of α and M^* are strongly correlated and so the errors quoted for α and M^* in the Table are conservatively large. We see a trend of faintening M^* and steepening α as EW (H α) increases. There is a significantly greater contrast between the H-high and H-mid samples than between the H-mid and H-low samples, despite the rather similar distribution of morphological types in the H-high and H-mid samples as compared with the H-low sample. This suggests that either there is not a simple one-to-one correlation between optical morphology and EW (H α), or that the larger fraction of Irr galaxies in the H-high sample are contributing to the steep faint-end slope for this sample.

Luminosity function estimates of the EW ([O II]) selected samples and errors in the best-fit Schechter parameters are shown in Figure 4. The 1σ error contours for the O-low and O-mid samples overlap and the O-high sample

Table 2. Luminosity function parameters.

Sample	$\langle V/V_{\max} \rangle$	α	M^*	\bar{n}	ϕ^*	ρ_L
(a) H-low	0.48 ± 0.01	-0.75 ± 0.28	-19.63 ± 0.24	10.1 ± 2.5	4.5 ± 1.1	5.9 ± 1.4
(b) H-mid	0.49 ± 0.01	-0.72 ± 0.29	-19.28 ± 0.23	11.0 ± 2.8	5.4 ± 1.4	5.1 ± 1.4
(c) H-high	0.54 ± 0.01	-1.28 ± 0.30	-19.04 ± 0.26	48.0 ± 15.9	8.5 ± 2.8	8.8 ± 2.9
(d) O-low	0.51 ± 0.01	-0.80 ± 0.29	-19.51 ± 0.22	13.8 ± 3.2	5.8 ± 1.3	6.8 ± 1.7
(e) O-mid	0.49 ± 0.01	-0.36 ± 0.34	-19.16 ± 0.22	7.4 ± 1.8	5.8 ± 1.3	4.9 ± 1.1
(f) O-high	0.51 ± 0.01	-1.49 ± 0.26	-19.49 ± 0.30	46.0 ± 15.9	3.7 ± 1.2	7.9 ± 2.8

α is the faint-end slope and M^* the characteristic b_J magnitude of the best-fit Schechter function. \bar{n} is the space density of galaxies in the range $-22 < M < -15$ and ϕ^* is the normalisation of the Schechter luminosity function, both in units of $10^{-3}h^3\text{Mpc}^{-3}$. ρ_L is the luminosity density integrated over the same magnitude range, in units of $10^7 L_{\odot}h^3\text{Mpc}^{-3}$.

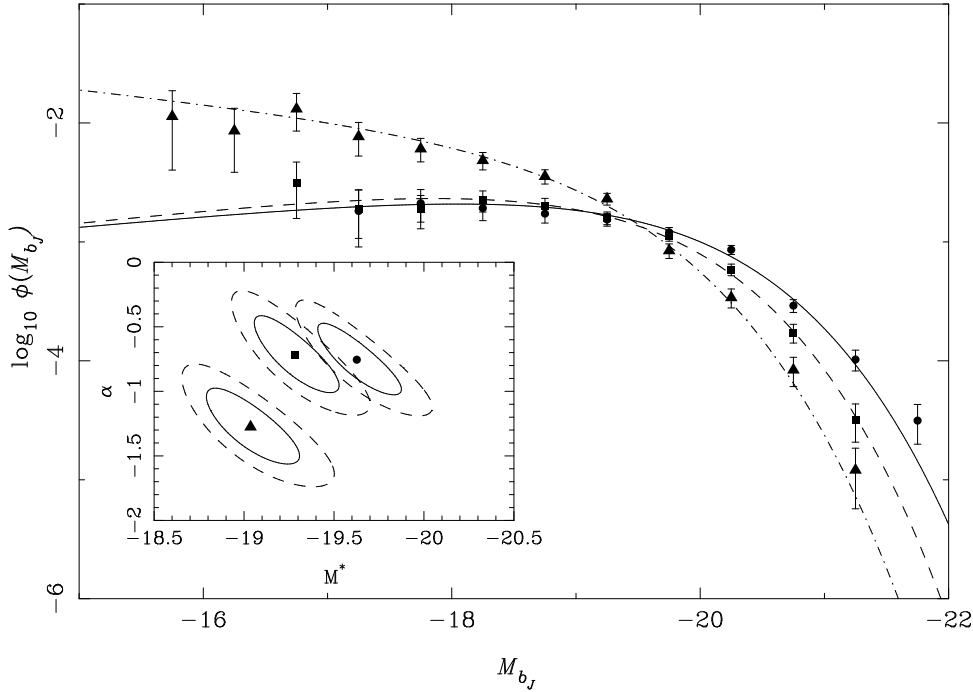


Figure 3. Estimates of the luminosity function for galaxies with no significant detected $\text{H}\alpha$ emission (H-low: circles, solid line), with moderate $\text{H}\alpha$ emission (H-mid: squares, dashed line) and with strong $\text{H}\alpha$ emission (H-high: triangles, dot-dashed line). The symbols with error bars show the stepwise fit, the curves show the Schechter function fits. For clarity, data points representing fewer than five galaxies have been omitted from the plot. The inset shows 1 & 2 σ likelihood contours for the best-fit Schechter parameters.

does not show a fainter M^* than non-emission line galaxies. However, the LF for the O-high sample does have a significantly steeper faint-end slope than that for galaxies with only weak or moderate $[\text{O II}]$ emission.

The fact that we see a systematic dimming of M^* with emission-line EW for the $\text{H}\alpha$ -selected sample but not for the $[\text{O II}]$ -selected sample is probably due to the fact that EW($\text{H}\alpha$) is a measure of the fraction of ionizing photons from OB stars over the flux from the old stellar population emitted in the rest-frame R band which forms the continuum at $\text{H}\alpha$, while EW($[\text{O II}]$) is normalised by the flux from relatively young stars (mainly type A). Thus EW($\text{H}\alpha$) is

more sensitive to the current star formation rate and hence blue luminosity enhancement than EW($[\text{O II}]$).

Note that the LF estimate for late-type galaxies presented by L92 does not have such a steep faint-end slope as we find here for strong emission-line galaxies. In L92 we combined galaxies classified as spiral or irregular as “late type”, and so not all of them have strong emission lines. The faint-end slope for early-type galaxies (L92) was much shallower than that measured here for galaxies with no emission lines. At least part of this difference is due to a bias in the morphological type dependent LFs of L92 due to the tendency of unclassified galaxies in the Stromlo-APM survey to be of low luminosity (Marzke et al. 1994, Zucca et al. 1994). We

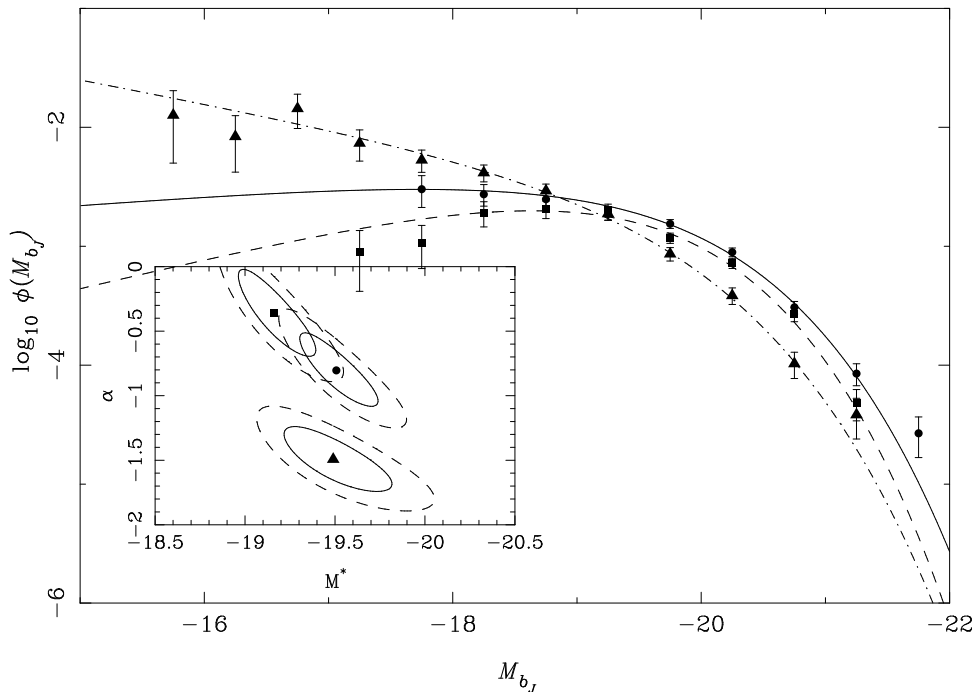


Figure 4. Estimates of the luminosity function for galaxies with no significant detected [O II] emission (O-low: circles, solid line), with moderate [O II] emission (O-mid: squares, dashed line) and with strong [O II] emission (O-high: triangles, dot-dashed line). The symbols with error bars show the stepwise fit, the curves show the Schechter function fits. For clarity, data points representing fewer than five galaxies have been omitted from the plot. The inset shows 1 & 2σ likelihood contours for the best-fit Schechter parameters.

avoid this bias with the spectroscopically selected samples analysed here.

The normalisation ϕ^* of the fitted Schechter functions was estimated using a minimum variance estimate of the space density \bar{n} of galaxies in each sample (Davis & Huchra 1982, L92). We corrected our estimates of \bar{n} , ϕ^* and luminosity density ρ_L to allow for those galaxies excluded from each subsample. First, all subsamples were scaled by the factor 1715/1660 to account for the 55 galaxies with no EW information available. Second, all H α selected subsamples were scaled by 1660/1578 to account for the 82 galaxies whose H α line, if present, would have fallen in the “red gap” (§2). Samples H-mid & H-high were scaled by an additional factor 1578/1521 to allow for the 57 galaxies in which H α was seen, but was not able to be measured. Finally, samples O-mid & O-high were scaled by 1660/1655 to allow for the five galaxies in which [O II] was seen but not measured. Our final estimates of \bar{n} , ϕ^* and ρ_L are given in Table 2. The uncertainty in mean density due to “cosmic variance” (L92 equation 7) is $\approx 6\%$ for each sample. However, the errors in these quantities are dominated by the uncertainty in the shape of the LF, particularly by the value of the estimated characteristic magnitude M^* .

Using both H α and [O II] equivalent widths as indicators of star formation activity, we find that galaxies currently undergoing significant bursts of star formation dominate the faint-end of the luminosity function, whereas more quiescent galaxies dominate at the bright end. This is in agreement with the results of Lin et al. (1996a) and Zucca et al.

(1997), but in disagreement with Salzer (1989), who finds no significant difference in the LF shapes of star-forming and quiescent galaxies. As pointed out by Schade & Ferguson (1994), Salzer’s sample is biased against weak-lined ELGs at low-luminosity, and their reanalysis of his data correcting for this selection effect does find a steep faint-end slope for the LF of star-forming galaxies.

The characteristic magnitude M^* for the O-high sample is about 0.5 mag brighter than that for the H-high sample. This is probably due to a combination of several factors: 1) A large [O II] EW can come from a small [O II] flux and a very red continuum (ie. a small star formation rate and an old stellar population). 2) The correlation between estimated values of faint-end slope α and characteristic magnitude M^* means that the steeper α of the O-high sample will push the estimated M^* to brighter magnitudes. 3) The errors on M^* are large (± 0.3 mag), and so the H-high and O-high M^* estimates disagree only at the 1–2 σ level.

4 GALAXY CLUSTERING

In this section we measure the clustering properties of the galaxy subsamples. We measure the auto-correlation function of each sample in redshift space, and the cross-correlation function of each galaxy sample with all galaxy types in real space. For both estimates, we first verified that the 194 galaxies missing EW (H α) measurement and the 60 galaxies missing EW ([O II]) did not bias the measured

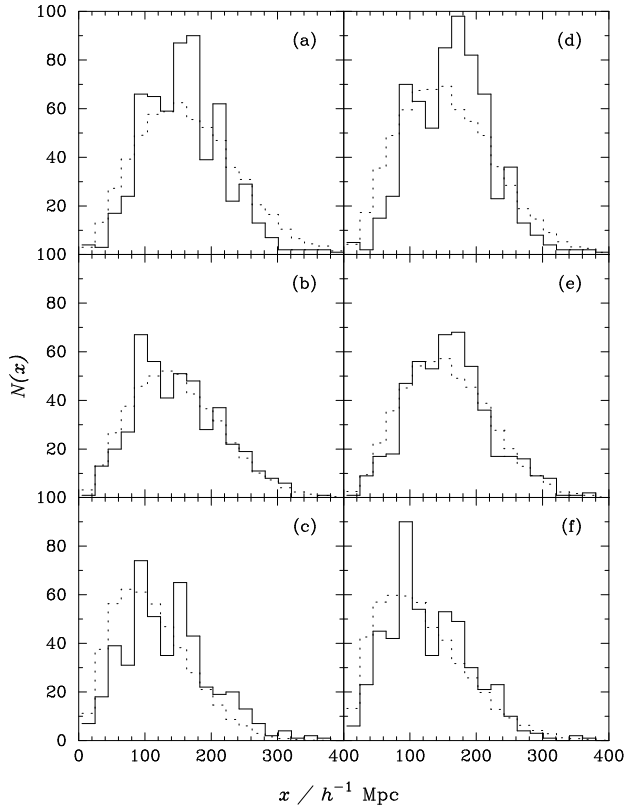


Figure 5. The solid histograms show the observed number-distance $N(x)$ distribution for each galaxy subsample defined in Table 1. The dashed lines show the expected distribution from our luminosity function fits.

clustering relative to the complete sample. Those galaxies excluded because H α fell in the “red gap” lie at redshifts $z \approx 0.06$ – 0.07 . Nevertheless, omitting these galaxies did not significantly affect the measured clustering in real or redshift space.

4.1 Redshift-Space Correlation Function

We correct for boundary conditions and the survey selection function by populating the survey volume with a catalogue of $\sim 18,000$ random points whose radial density matches that expected for each subsample. The number-distance distributions for the six galaxy subsamples analysed here are shown in Figure 5. These plots also show the expected distributions inferred from the luminosity functions calculated in the previous section. We see that given the tendency for non-ELGs to be luminous and for ELGs to be faint, the ELGs are slightly overdense at large distances ($x \gtrsim 200h^{-1}\text{Mpc}$) whereas there is an underdensity of non-ELGs at similar distances. This observation is reflected by the increasing $\langle V/V_{\text{max}} \rangle$ with EW (H α) seen in Table 2, and is probably due to evolution in emission line strength with redshift (eg. Broadhurst et al. 1992), occurring at redshifts as low as $z \lesssim 0.15$. It is unlikely to be due to the changing pro-

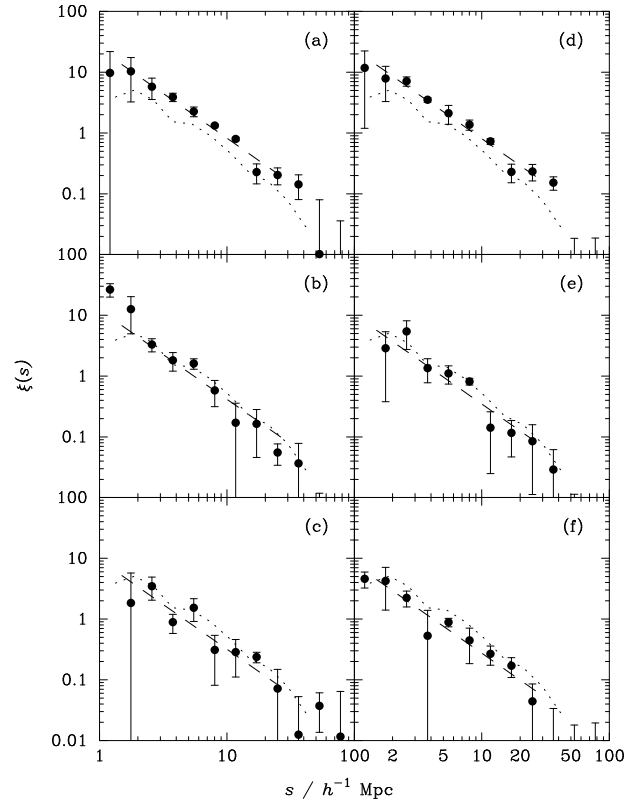


Figure 6. Estimates of the redshift-space correlation function for the galaxy samples given in Table 1. Error bars show the rms variance from dividing the survey into 4 distinct zones. The dashed line shows the best-fit power-law over the range 1.5 – $30 h^{-1}\text{Mpc}$ with the index held fixed at $\gamma_s \equiv 1.47$. The dotted line shows $\xi(s)$ estimated from the full Stromlo-APM sample (Loveday et al. 1995).

jected size of the spectrograph slit at different redshifts as we demonstrated in Paper 1. We checked that these discrepancies between observed and expected $N(x)$ distributions did not bias our estimates of $\xi(s)$ by also generating a random distribution according to a fourth-order polynomial fit to the observed radial density of each subsample. Clustering estimates using this random distribution gave results consistent with a random distribution generated according to the predicted radial density.

The auto-correlation function of each sample in redshift space is measured using the estimator

$$1 + \xi(s) = \frac{w_{gg}(s)w_{rr}(s)}{[w_{gr}(s)]^2}, \quad (2)$$

Hamilton (1993). Here $w_{gg}(s)$, $w_{gr}(s)$ and $w_{rr}(s)$ are the summed products of the weights of galaxy-galaxy, galaxy-random and random-random pairs respectively at separation s . We use the minimum-variance pair weighting given by equation 1 of Loveday et al. (1995), and the reader is referred to that paper for further details. Errors are estimated by dividing the survey into four zones of roughly equal area and calculating the variance in $\xi(s)$ from zone-to-zone.

Table 3. Correlation function parameters.

Sample	s_0	γ_r	r_0
(a) H-low	8.7 ± 0.5	1.78 ± 0.08	6.0 ± 1.4
(b) H-mid	5.5 ± 0.7	1.60 ± 0.13	5.2 ± 2.0
(c) H-high	4.6 ± 0.9	1.87 ± 0.16	2.9 ± 1.9
(d) O-low	8.6 ± 1.1	1.79 ± 0.07	6.2 ± 1.8
(e) O-mid	4.9 ± 0.6	1.64 ± 0.05	4.7 ± 0.8
(f) O-high	4.1 ± 0.9	1.78 ± 0.15	2.9 ± 0.7

s_0 is the correlation length measured in redshift space over the range $1.5\text{--}30 h^{-1}\text{Mpc}$ with the power-law index held fixed at $\gamma_s \equiv 1.47$. γ_r and r_0 are the real-space power-law parameters over $0.2\text{--}20 h^{-1}\text{Mpc}$ determined from cross-correlation with the 2d APM survey (§4.2).

Estimates of $\xi(s)$ are shown in Figure 6. A power-law $\xi(s) = (s/s_0)^{-\gamma_s}$ was fitted over the range $1.5\text{--}30 h^{-1}\text{Mpc}$. For each subsample the estimated power-law slope γ_s was formally consistent with $\gamma_s = 1.47$, measured for the whole Stromlo-APM sample (Loveday et al. 1995). Since estimates of the index γ_s and correlation length s_0 are strongly correlated, we determined the best fit s_0 to each subsample, keeping the power-law index fixed at $\gamma_s = 1.47$. The results of these fits are shown by the dashed lines in Figure 6 and the best-fit values of s_0 with 1σ uncertainties (determined from fitting to each zone separately) are shown in Table 3.

We see that the correlation length s_0 becomes significantly smaller in more actively star-forming galaxies, as traced by both EW ($\text{H}\alpha$) and EW ($[\text{O II}]$). This result is in agreement with the power-spectrum analysis of the Las Campanas Redshift Survey by Lin et al. (1996b) who find that the clustering amplitude of ELGs is only about 70% that of the full LCRS sample. These results are also consistent with those of Rosenberg et al. (1994), Iovino et al. (1988) and Salzer (1989), all of whom find that ELGs are less strongly clustered than quiescent galaxies. Galaxies with no detected $\text{H}\alpha$ (H-low) or $[\text{O II}]$ (O-low) emission have a correlation length about twice that of ELG galaxies (H-high and O-high samples). This is larger than the difference in clustering amplitude determined by Lin et al. (1996b) from the LCRS, presumably because we have subdivided galaxies into three EW bins compared to their two EW bins.

4.2 Real-Space Correlation Function

The estimate of $\xi(s)$ described above is affected by redshift space distortions. On small scales, random, thermal motions tend to decrease galaxy clustering, whereas on large scales, galaxy streaming motions tend to enhance $\xi(s)$. In order to avoid the effects of galaxy peculiar velocities, we have calculated the projected cross-correlation function $\Xi(\sigma)$ of each galaxy subsample with all galaxies in the APM survey to a magnitude limit of $b_J = 17.15$. We then invert this projected correlation function to obtain the real space cross-correlation function $\xi(r)$ of each subsample with the full galaxy sample. This method of estimating $\xi(r)$ is described by Saunders et al. (1992) and by Loveday et al. (1995).

The large number of galaxy pairs used by this estimator allows us to fit a power-law to the measured cross-correlation function over the range of separations $0.2\text{--}20 h^{-1}\text{Mpc}$ and to fit both the power-law index γ_r and the correlation length r_0 .

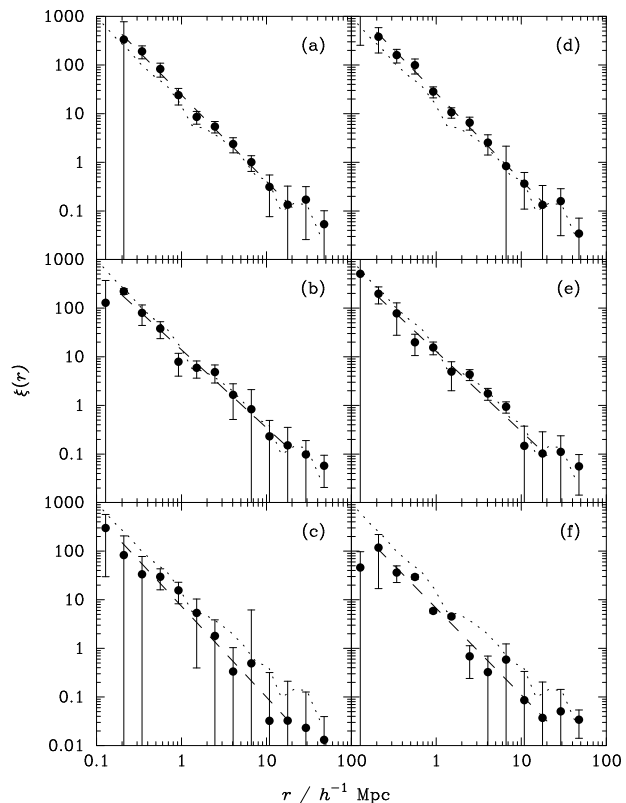


Figure 7. Estimates of the real-space correlation function for the galaxy samples given in Table 1. Error bars show the rms variance from dividing the survey into 4 distinct zones. The dashed line shows the best-fit power-law over the range $0.2\text{--}20 h^{-1}\text{Mpc}$. The dotted line shows $\xi(r)$ estimated from the full Stromlo-APM sample (Loveday et al. 1995).

Our estimates of $\xi(r)$ are plotted in Figure 7 and our best-fit power-laws are tabulated in Table 3. As in redshift-space, we see that strong emission-line galaxies are more weakly clustered than their quiescent counterparts by a factor of about two.

The real space clustering measured for non-ELGs is very close to that measured for early-type (E + S0) galaxies, and the clustering of late-type (Sp + Irr) galaxies lies between that of the moderate and high EW galaxies (cf. Loveday et al. 1995). Given the strong correlation between morphological type and presence of emission lines (Table 1) this result is not unexpected. The power-law slopes are consistent ($\gamma_r = 1.8 \pm 0.1$) between the H-low, H-high, O-low and O-high samples. For the moderate EW galaxies (H-mid and O-mid samples) we find shallower slopes ($\gamma_r = 1.6 \pm 0.1$). This is only a marginally significant (1–2 σ) effect, but may indicate a deficit of moderately star-forming galaxies principally in the cores of high density regions, whereas strongly star forming galaxies appear to more generally avoid overdense regions.

5 CONCLUSIONS

We have presented the first analysis of the luminosity function and spatial clustering for representative and well-defined local samples of galaxies selected by EW ($H\alpha$), the most direct tracer of star-formation. We have also selected galaxies by EW ($[O\ II]$), and find broadly consistent results between the two tracers of star formation, which is expected from their close relation (Kennicutt 1992, Paper 1). The observed trend for M^* to fainten systematically with increasing EW ($H\alpha$), contrasted with the roughly constant M^* with varying EW ($[O\ II]$), is probably due to EW ($H\alpha$) being a more reliable indicator of star formation rate than EW ($[O\ II]$).

Star-forming galaxies are likely to be significantly fainter than their quiescent counterparts. The faint-end ($M \gtrsim M^*$) of the luminosity function is dominated by ELGs and thus the majority of local dwarf galaxies are currently undergoing star formation.

Star-forming galaxies are more weakly clustered, both amongst themselves, and with the general galaxy population, than quiescent galaxies. This weaker clustering is observable on scales from 0.1–10 h^{-1} Mpc. We thus confirm that star-forming galaxies are preferentially found today in low-density environments.

A possible explanation for these observations is that luminous galaxies in high-density regions have already formed all their stars by today, while less luminous galaxies in low-density regions are still undergoing star formation. It is not clear what might be triggering the star formation in these galaxies today. While interactions certainly enhance the rate of star formation in some disk galaxies, interactions with luminous companions can only account for a small fraction of the total star formation in disk galaxies today (Kennicutt et al. 1987). Telles & Maddox (1999) have investigated the environments of $H\ II$ galaxies by cross-correlating a sample of $H\ II$ galaxies with APM galaxies as faint as $b_J = 20.5$. They find no excess of companions with $H\ I$ mass $\gtrsim 10^8 M_\odot$ near $H\ II$ galaxies, thus arguing that star formation in most $H\ II$ galaxies is unlikely to be induced by even a low-mass companion.

Our results are entirely consistent with the hierarchical picture of galaxy formation. In this picture, today's luminous spheroidal galaxies formed from past mergers of galactic sub-units in high density regions, and produced all of their stars in a merger induced burst, or series of bursts, over a relatively short timescale. The majority of present-day dwarf, star-forming galaxies in lower density regions may correspond to unmerged systems formed at lower peaks in the primordial density field (eg. Bardeen et al. 1986) and whose star formation is still taking place. Of course, the full picture of galaxy formation is likely to be significantly more complicated than this simple sketch, and numerous physical effects such as depletion of star-forming material and other feedback mechanisms are likely to play an important role.

ACKNOWLEDGMENTS

We thank George Efstathiou and Bruce Peterson for their contributions to the Stromlo-APM survey.

REFERENCES

- Bardeen, J.M., Bond, J.R., Kaiser, N. & Szalay, A.S., 1986, *ApJ*, 304, 15
- Brinchmann, J., et al., 1998, *ApJ*, 499, 112
- Broadhurst, T.J., Ellis, R.S. & Glazebrook, K., 1992, *Nature*, 355, 55
- Bromley, B.C., Press, W.H., Lin, H., & Kirshner, R.P., 1998, *ApJ*, 505, 25
- Davis, M. & Geller, M.J., 1976, *ApJ*, 208, 13
- Davis, M. & Huchra, J., 1982, *ApJ*, 254, 437
- Efstathiou, G., Ellis, R.S. & Peterson, B.A., 1988, *MNRAS*, 232, 431
- Folkes, S.R., et al, 1999, *MNRAS*, in press (astro-ph/9903456)
- Giovanelli, R., Haynes, M.P. & Chincarini, G.L., 1986, *ApJ*, 300, 77
- Hamilton, A.J.S., 1993, *ApJ*, 417, 19
- Iovino, A., Melnick, J. & Shaver, P., 1988, *ApJL*, 330, L17
- Iovino, A., Giovanelli, R., Haynes, M., Chincarini, G. & Guzzo, L., 1993, *MNRAS*, 265, 21
- Kennicutt, R.C. 1983, *ApJ*, 272, 54
- Kennicutt, R.C. 1992, *ApJ*, 388, 310
- Kennicutt, R.C., Keel, W.C., van der Hulst, J.M., Hummel, E. & Roettiger, K.A., 1987, *AJ*, 93, 1011
- Lin, H., et al., 1996a, *ApJ*, 464, 60
- Lin, H., et al., 1996b, *ApJ*, 471, 617
- Loveday, J., 1996, *MNRAS*, 278, 1025
- Loveday, J., Peterson, B.A., Efstathiou, G. & Maddox, S.J., 1992, *ApJ*, 390, 338 (L92)
- Loveday, J., Maddox, S.J., Efstathiou, G., & Peterson, B.A., 1995, *ApJ*, 442, 457
- Loveday, J., Peterson, B.A., Maddox, S.J., & Efstathiou, G., 1996, *ApJS*, 107, 201
- Marzke, R.O., Geller, M.J., Huchra, J.P. & Corwin, H.G., 1994, *AJ*, 108, 437
- Marzke, R.O., da Costa, L.N., Pellegrini, P.S., Willmer, C.N.A. & Geller, M.J., 1998, *ApJ*, 503, 617
- Rosenberg, J.L., Salzer, J.J., & Moody, J.W., 1994, *AJ*, 108, 1557
- Salzer, J.J., 1989, *ApJ*, 347, 152
- Sandage, A., Tammann, G.A. & Yahil, A., 1979, *ApJ*, 232, 352
- Saunders, W., Rowan-Robinson, M. & Lawrence, A., 1992, *MNRAS*, 258, 134
- Schade, D.J., & Ferguson, H.C., 1994, *MNRAS*, 267, 889
- Schechter, P.L., 1976, *ApJ*, 203, 297
- Telles, E., Maddox, S., 1999, submitted to *MNRAS*
- Tresse, L., Maddox, S.J., Loveday, J., & Singleton, C., 1999, *MNRAS*, in press (Paper 1)
- Zucca, E., Pozzetti, L. & Zamorani, G., 1994, *MNRAS*, 269, 953
- Zucca, E., et al., 1997, *A&A*, 326, 477